On Three-Dimensional ALE Finite Element Model For Simulating Interstitial Medium Deformation in the Presence of a Moving Needle

Yannick Deleuze, Marc Thiriet, Tony W.H. Sheu

On Three-Dimensional ALE Finite Element Model For Simulating Interstitial Medium Deformation in the Presence of a Moving Needle

Yannick Deleuze, Marc Thiriet, and Tony Sheu

Abstract The effects of inserted needle on the subcutaneous interstitial flow is studied. A goal is to describe the physical stress affecting cells during acupuncture needling. The convective Brinkman equations are considered to describe the flow through a fibrous medium. Three-dimensional simulations are carried out employing an ALE finite element model. Numerical studies illustrate the acute physical stress developed by the implantation of a needle.

1 Introduction

In recent years, computational techniques have been widely used by researchers to investigate and simulate biological flow within three dimensional context. Applications include blood flow models, air flow models in the respiratory tract, interstitial

Yannick Deleuze
Sorbonne Universités, UPMC Univ Paris 06, UMR 7598, Laboratoire Jacques-Louis Lions, F-75005, Paris, France
Department of Engineering Science and Ocean Engineering, National Taiwan University, No. 1, Sec. 4, Roosevelt Road, Taipei, Taiwan e-mail: yannick.deleuze@ljll.math.upmc.fr

Marc Thiriet
CNRS, UMR 7598, Laboratoire Jacques-Louis Lions, F-75005, Paris, France
Sorbonne Universités, UPMC Univ Paris 06, UMR 7598, Laboratoire Jacques-Louis Lions, F-75005, Paris, France
INRIA-Paris-Rocquencourt, EPC REO, Domaine de Voluceau, BP105, 78153 Le Chesnay Cedex
e-mail: marc.thiriet@upmc.fr

Tony W.H. Sheu
Department of Engineering Science and Ocean Engineering, National Taiwan University, No. 1, Sec. 4, Roosevelt Road, Taipei, Taiwan
Center for Advanced Study in Theoretical Sciences, National Taiwan University, No. 1, Sec. 4, Roosevelt Road, Taipei, Taiwan e-mail: twhsheu@ntu.edu.tw

flow models, and chemical mediators transport. Most of the structure and fluid interactions have been considered with simplified rigid wall or deformable wall models.

Methods to predict flows that account for moving domains or domain deformability using the finite element method are based on fixed mesh methods or moving mesh methods. On the one hand, fixed mesh methods include the immersed boundary formulation and the fictitious domain formulation. These methods are well adapted to moving bodies in the fluid or fluid-structure computation with interface of a highly geometric complexity. On the other hand, moving mesh methods include the Lagrangian method, the moving finite element (MFE) method, the deformation map method, the Geometric Conservation Law (GCL) method, the space/time finite element method, and the Arbitrarily Lagrangian–Eulerian (ALE) method for the solution of fluid dynamic problems.

The mathematically rigorous ALE framework has been well accepted to be applicable to simulate transport phenomena in time and allows some freedom in the description of mesh motion. A theoretical analysis of the ALE method can be found in [5, 8]. However, ALE equations are computationally expensive when considering a large domain because of the necessity of continuously updating the geometry of the fluid and structural mesh. Interface tracking with time discretization also raises some implementation questions. The implementation of the ALE method can be done in FreeFem++ [2].

Study of biological flows plays a central role in acupuncture research. For a description of the underlying acupuncture mechanism, one can refer to [3, 14, 15]. Interstitial flow models take into account interstitial fluid, cell membrane interaction, and fiber interactions [10]. Mastocytes, among other cells, are able to respond to fluidic stimuli via mechanotransduction pathways leading to the degranulation and liberation of chemical mediators [7]. Degranulation mechanisms include interaction of the cell membrane with interstitial and cytosolic flow [16]. Ion transport in narrow ion channels is another challenging task to model. Indeed, degranulation of chemical mediators upon stimulation can be triggered by a rapid Ca^{2+} entry in the cytosol [12].

Modeling the three-dimensional interstitial flow in tissues is extremely challenging for a large number of reasons: a complex geometry of the tissue, an accurate constitutive description of the behavior of the tissue, and flow rheology are only a few examples. Macroscopic models for incorporating complex microscopic structure are essential for applications [1, 10, 12, 19, 20]. In the context of acupuncture, the interstitial flow has been modeled by the Brinkman equations [3, 19, 20].

In this paper, a porous medium formulation of the interstitial fluid is presented for modeling mastocyte-needle interaction in deformable connective tissues. This formulation is based on a conventional ALE characteristic/Galerkin finite element model for an unsteady flow thought a porous medium modeled by the incompressible Brinkman's equations in a three-dimensional moving domain. The motion of the needle in the fluid is taken into account. The main features of the model can be summarized as follows:

1. The loose connective tissue of the hypodermis is constituted of scattered cells immersed in extracellular matrix. The extracellular matrix contains relatively sparse

fibers and abundant interstitial fluid. The interstitial fluid contains water, ions and other small molecules. Such a fluid corresponds to plasma without macromolecules and interacts with the ground substance, thereby forming a viscous hydrated gel that can stabilize fiber network [11, 13].
2. The Darcys law is used to approximate fibers of the media as a continuum and allows us to compute the actual microscopic flow phenomena that occur in the fibrous media.
3. Brinkman's law then allows us to describe the flow field around solid bodies such as the embedded cells in extracellular matrix.
4. Transient convective Brinkman's equations are applied to simulate the interstitial flow in a fibrous medium driven by a moving needle.

Although the previously stated approach cannot give information on microscopic events, it can describe macroscale flow patterns in porous media. Focus is given to the effects of interstitial fluid flow during implantation of an acupuncture needle until the tip has reached the desired location within the hypodermis. The objective of this work is to give a description of the physical stress (shear stress and pressure) influencing tissue and cells.

2 Methods

Due to biological complexity, the interstitium is considered as a fluid-filled porous material. The interstitial flow is simulated using the incompressible convective Brinkman equation.

2.1 Flow equations

The governing equations of the unsteady flow of an incompressible fluid through a porous medium (with mass density ρ, dynamic viscosity μ, and kinematic viscosity $\nu = \mu/\rho$) can be derived as [17]:

$$\frac{\rho}{\alpha_f}\left(\frac{\partial \bar{\mathbf{u}}}{\partial t} + \bar{\mathbf{u}}\cdot\nabla\left(\frac{\bar{\mathbf{u}}}{\alpha_f}\right)\right) - \mu\nabla^2\bar{\mathbf{u}} + \frac{1}{\alpha_f}\nabla(\alpha_f p_f) = -\frac{\mu}{P}\bar{\mathbf{u}} \quad \text{in } \Omega(t), \tag{1}$$

$$\nabla\cdot\bar{\mathbf{u}} = 0, \tag{2}$$

$$\bar{\mathbf{u}}(\mathbf{x},0) = \bar{\mathbf{u}}_0(\mathbf{x}), \tag{3}$$

where $-\frac{\mu}{P}\bar{\mathbf{u}}$ denotes the Darcy drag, P the Darcy permeability, $\bar{\mathbf{u}}$ the averaged velocity vector, and p_f the pressure. The averaged velocity is defined as

$$\bar{\mathbf{u}} = \alpha_f \mathbf{u}_f, \tag{4}$$

where $\mathbf{u}_f$ is the fluid velocity and

$$\alpha_f = \frac{\text{fluid volume}}{\text{total volume}} \tag{5}$$

is the fluid volume fraction. This volume fraction corresponds to the effective porosity of the medium. The fluid fractional volume α_f is taken as a space-dependent parameter to model the distinguished properties of an acupoint.

The system of equations (1-2) is applied to the case of a flow driven by the motion of a needle in the deformable domain $\Omega(t)$ [3]. The domain boundary can be decomposed into three surfaces: the needle boundary denoted by Γ_1, an impervious boundary (wall) denoted by Γ_2, the mastocyte membrane denoted by Γ_3 and the open boundary on the sides denoted by Γ_4. The classical no-slip condition is applied to the needle surface Γ_1, the rigid wall Γ_2, and the cell surface Γ_3. At the outer boundary Γ_4 a traction-free boundary condition is prescribed. Thus, the entire set of boundary conditions reads as

$$\bar{\mathbf{u}} = \mathbf{v}_{\text{needle}}, \text{ on } \Gamma_1, \tag{6}$$
$$\bar{\mathbf{u}} = 0, \text{ on } \Gamma_2, \tag{7}$$
$$\bar{\mathbf{u}} = 0, \text{ on } \Gamma_3, \tag{8}$$
$$-\mu\nabla\bar{\mathbf{u}}\cdot\mathbf{n} + p_f\mathbf{n} = 0, \text{ on } \Gamma_4. \tag{9}$$

2.2 Finite element model

The governing equations in section 2.2.1 are solved using the finite element software FreeFem++ [6]. This code programs the discrete equations derived from the finite element weak formulation of the problem presented in section 2.2.3 using a characteristic/Galerkin model to stabilize convection terms.

2.2.1 Scaling and setting for numerical simulations

L denotes the characteristic length that is the needle width and V is the characteristic velocity set to be the needle maximum velocity. Rescaling the variables leads to

$$\mathbf{x}' = \frac{\mathbf{x}}{\mathsf{L}},\ t' = \frac{t}{(\mathsf{L}/\mathsf{V})},\ p' = \frac{p_f}{(\rho\mathsf{V}^2)},\ \mathbf{u}' = \frac{\bar{\mathbf{u}}}{\mathsf{V}}. \tag{10}$$

In the resulting dimensionless form, after removing the prime in the rescaled variables, the dimensionless incompressible convective Brinkman equations read as

$$\frac{1}{\alpha_f}\frac{\partial\mathbf{u}}{\partial t} + \frac{1}{\alpha_f}\mathbf{u}\cdot\nabla\left(\frac{\mathbf{u}}{\alpha_f}\right) - \frac{1}{\mathrm{Re}}\nabla^2\mathbf{u} + \frac{1}{\alpha_f}\nabla(\alpha_f p) = -\frac{1}{\mathrm{Da}\,\mathrm{Re}}\mathbf{u}, \tag{11}$$
$$\nabla\cdot\mathbf{u} = 0. \tag{12}$$

where Re is the Reynolds number and Da is the Darcy number. The previous dimensionless parameters are defined as

$$\mathrm{Re} = \frac{\rho \mathsf{L}\mathsf{V}}{\mu},\ \mathrm{Da} = \frac{\mathscr{P}}{\mathsf{L}^2}. \tag{13}$$

In considering the above dimensionless governing equations, the normalized boundary conditions on the domain boundary are prescribed as

$$\mathbf{u} = \mathbf{v} \ \text{ on } \Gamma_1, \tag{14}$$

$$\mathbf{u} = 0 \ \text{ on } \Gamma_2, \tag{15}$$

$$\mathbf{u} = 0 \ \text{ on } \Gamma_3, \tag{16}$$

$$-\frac{1}{\mathrm{Re}}\nabla\mathbf{u}\cdot\mathbf{n} + p\mathbf{n} = 0 \ \text{ on } \Gamma_{sides}. \tag{17}$$

2.2.2 ALE implementation on moving meshes

In the present paper, the ALE framework built in FreeFem++ is employed to compute the flow in the moving domain. In the current problem setting, the motion of needle is prescribed with respect to time. The boundary of the domain is thus exactly known at each time so that an area preserving mesh can be precisely generated.

The framework of the ALE approach employed is briefly described below. Let $\Omega(t)$ be the domain at each time t with regular boundary $\partial\Omega(t)$. In the Eulerian description, the fluid is described by

$$\mathbf{u}(\mathbf{x},t) \text{ and } p(\mathbf{x},t), \forall \mathbf{x} \in \Omega(t). \tag{18}$$

To follow a moving domain, one can define the ALE map as

$$\tilde{\mathscr{A}} : \tilde{\omega} \times \mathbb{R}^+ \to \mathbb{R}^2 \quad (\tilde{\mathbf{x}},t) \to \tilde{\mathscr{A}}(\tilde{\mathbf{x}},t) := \tilde{\mathscr{A}}_t, \tag{19}$$

such that $\omega(t) = \tilde{\mathscr{A}}(\tilde{\omega},t)$, where $\tilde{\omega}$ is the reference computational domain. Given an ALE field $\tilde{q} : \tilde{\omega} \times \mathbb{R}^+ \to \mathbb{R}$, its Eulerian description is given by

$$\forall \mathbf{x} \in \Omega(t), q(\mathbf{x},t) = \tilde{q}(\tilde{\mathscr{A}}_t^{-1}(\mathbf{x}),t) \tag{20}$$

In ALE framework, the computational domain velocity (or ALE velocity or grid velocity) is defined as

$$\tilde{\mathbf{a}}(\tilde{\mathbf{x}},t) = \frac{\partial \tilde{\mathscr{A}}}{\partial t}(\tilde{\mathbf{x}},t), \quad \forall \tilde{\mathbf{x}} \in \tilde{\omega}, \tag{21}$$

so that we can get

$$\mathbf{a}(\mathbf{x},t) = \tilde{\mathbf{a}}(\tilde{\mathscr{A}}_t^{-1},t). \tag{22}$$

The ALE time-derivative is defined as

$$\left.\frac{\partial q}{\partial t}\right|_{\mathscr{J}} = \frac{\mathrm{d}}{\mathrm{d}t} q(\mathscr{J}(\tilde{\mathbf{x}},t),t), \tag{23}$$

and the following identity holds

$$\left.\frac{\partial q}{\partial t}\right|_{\mathscr{J}} = (\mathbf{a}.\nabla)q + \frac{\partial q}{\partial t}. \tag{24}$$

A general method is used to construct the mapping or, equivalently, the domain velocity **a**. The domain velocity is computed by solving the following Laplace equation subjected to the Dirichlet boundary condition [4]

$$-\nabla^2 \mathbf{a} = 0, \qquad \mathbf{a}_{|\partial\Omega} = \mathbf{v}. \tag{25}$$

In the ALE framework, the equations (11-12), subject to a prescribed needle motion, become

$$\left.\frac{\partial(\mathbf{u}/\alpha_f)}{\partial t}\right|_{\mathscr{J}} + \left(\left(\frac{\mathbf{u}}{\alpha_f} - \mathbf{a}\right)\cdot\nabla\right)\frac{\mathbf{u}}{\alpha_f} - \frac{1}{\mathrm{Re}}\nabla^2\mathbf{u} + \frac{1}{\alpha_f}\nabla(\alpha_f p) = -\frac{\mathbf{u}}{\mathrm{Da}\,\mathrm{Re}}, \tag{26}$$

$$\nabla\cdot\mathbf{u} = 0. \tag{27}$$

The solutions **u** and p are sought subject to the initial condition (3) and the boundary conditions (7-9) described in section 2.2.1.

2.2.3 Finite element discretization

The convective incompressible Brinkman equations are approximated with the method of characteristics for the nonlinear convection term and a Galerkin method for the rest of the spatial derivative terms. The time discretization gives

$$\frac{1}{\Delta t}\left(\frac{\mathbf{u}^{n+1}}{\alpha_f} - \left(\frac{\mathbf{u}^n}{\alpha_f}\right)\circ\mathbf{X}^n\right) - \frac{1}{\mathrm{Re}}\nabla^2\mathbf{u}^{n+1} + \frac{1}{\alpha_f}\nabla(\alpha_f p^{n+1}) = -\frac{\mathbf{u}^{n+1}}{\mathrm{Da}\,\mathrm{Re}}, \tag{28}$$

$$\nabla\cdot\mathbf{u}^{n+1} + \varepsilon p^{n+1} = 0, \tag{29}$$

in Ω^{n+1}. Note that $\mathbf{X}^n$ is approximated by $\mathbf{X}^n \approx \mathbf{x} - \left(\frac{\mathbf{u}^n}{\alpha_f} - \mathbf{a}^n\right)(\mathbf{x})\,\Delta t$. A small stabilization parameter ε is introduced following the so-called artificial compressibility method.

For all $\varphi \in H^{1/2}(\Gamma_1)$, let us introduce the product space

$$V_\varphi = \left\{(\mathbf{w},q) \in [H^1(\Omega)]^2 \times L^2(\Omega), \mathbf{w} = \varphi \text{ on } \Gamma_{\text{needle}}, \mathbf{w} = 0 \text{ on } \Gamma_{\text{wall}}\right\}. \tag{30}$$

Let

$$(a,b) = \int_{\Omega^{n+1}} ab\,\mathrm{d}\mathbf{x}. \tag{31}$$

The weak formulation becomes the following finite dimensional linear system: find $(\mathbf{u}^{n+1}, p^{n+1}) \in V_g$ such that

$$\begin{aligned} \frac{1}{\Delta t}\left(\frac{\mathbf{u}^{n+1}}{\alpha_f} - \left(\frac{\mathbf{u}^{n}}{\alpha_f}\right)\circ \mathbf{X}^n, \mathbf{w}\right) + \frac{1}{\mathrm{Re}}\left(\frac{1}{\alpha_f}\nabla \mathbf{u}^{n+1}, \nabla \mathbf{w}\right) \\ - \left(\alpha_f\, p^{n+1}, \nabla\cdot\left(\frac{\mathbf{w}}{\alpha_f}\right)\right) + \frac{1}{\mathrm{Da}\,\mathrm{Re}}\left(\mathbf{u}^{n+1}, \mathbf{w}\right) = 0, \\ \left(\nabla\cdot\mathbf{u}^{n+1}, q\right) + \varepsilon\left(p^{n+1}, q\right) = 0, \end{aligned} \tag{32}$$

for all $(\mathbf{w}, q) \in V_0$.

The Taylor-Hood $\mathbb{P}_2$–$\mathbb{P}_1$ elements are adopted to ensure satisfaction of the LBB stability condition [9]. Note that temporal accuracy order of the presented characteristic/Galerkin method is one. Meshes are generated within FreeFem++ and mesh adaptation is performed prior to simulations so as to enhance mesh quality around the needle and the cell.

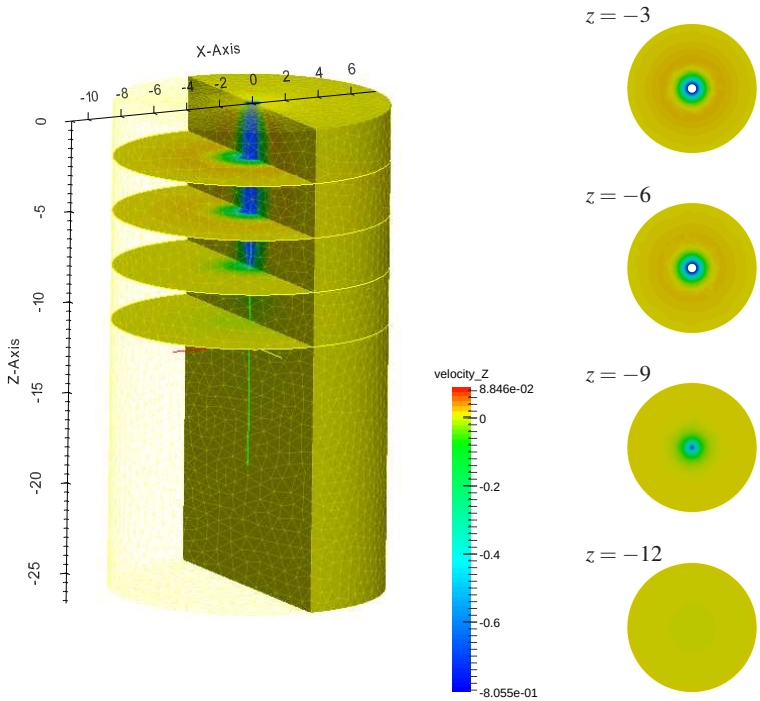

Fig. 1 The predicted contours of velocity along the z-direction resulting from the needle (blue) motion in interstitial fluid.

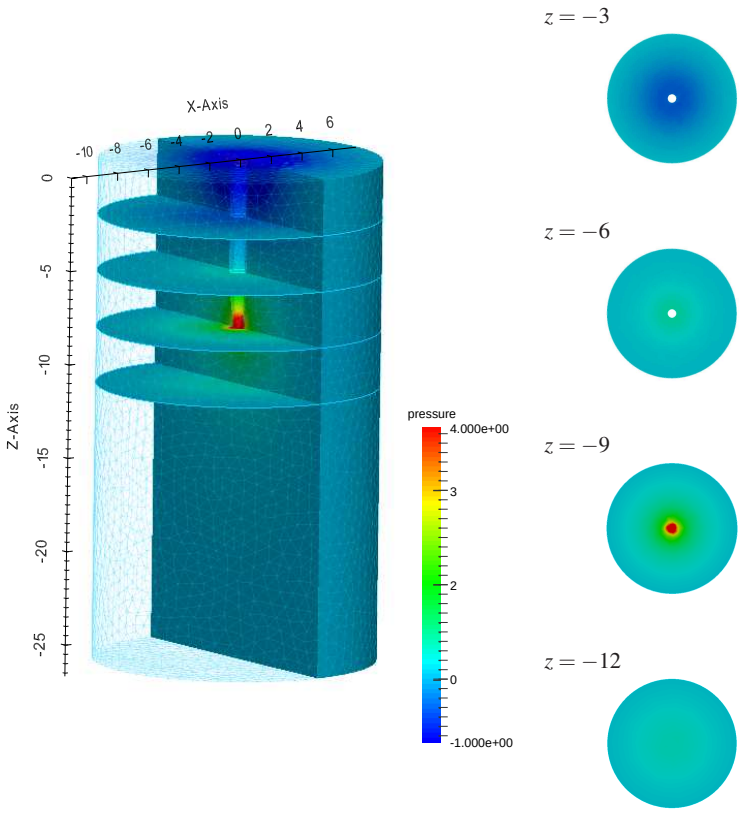

Fig. 2 The predicted contours of velocity along the z-direction resulting from the needle (blue) motion in interstitial fluid.

3 Results

In the present work, the needling direction is perpendicular to the skin surface. In practice, it is possible that the needling direction is oblique to the skin surface. The simulation results show that the insertion of an acupuncture needle can influence interstitial fluid flow. The computed velocity field shows that at a location away from the needle, the effect of the stress field vanishes (Fig. 1). Furthermore, when the needle reaches its maximum speed, the interstitial pressure gradient becomes higher at a location close to the needle tip (Fig. 2). The changes in the interstitial fluid flow and the high pressure gradient can affect the activities of the mastocyte pools in the stimulated area.

Another subject of interest is the effects of the fluidic stimuli on an interstitial cell. Local mechanical forces can trigger the activation of mechanoresponsive proteins on the cell surface [14, 18] so that Ca^{++} is allowed to enter the cytosol via

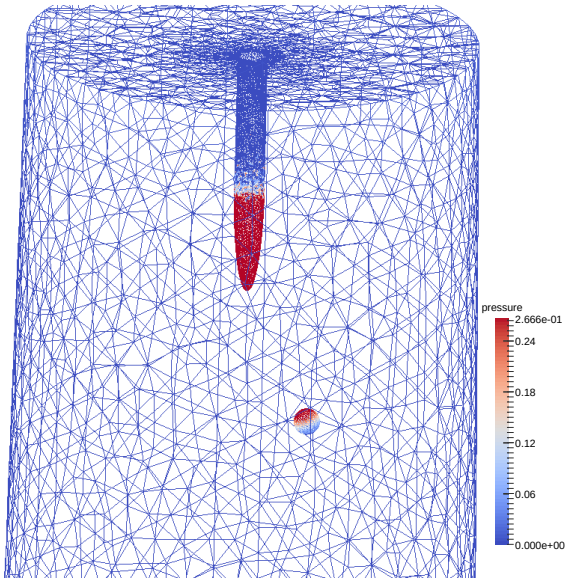

Fig. 3 The predicted pressure contours on the needle and cell surfaces as the needle moves toward the cell.

pressure and shear stress gated ion channels. Simulations are carried out by considering fixed cells and no-slip boundary condition prescribed at the cell surface. Figure 3 shows the pressure contours on the surface of a cell added closely to the needle. The pressure on the cell surface is higher in the region closest to the needle tip.

4 Conclusions

The proposed three-dimensional ALE finite element model is able to describe the interstitial flow and pressure from the macroscopic point of view when a needle is inserted and moving within the hypodermis. High local fluid pressure and shear stress on cells are most likely to appear near the needle tip region. However, the proposed method does not allow the rotation of the needle to be taken into account. When considering the rotation of the needle, a large deformation of the tissue is observed with the twisting of the fibers around the needle, that in turn makes the corresponding change in interstitial flow. A fluid/structure model taking into account the mechanics of the fibers should then be considered. This study has shown that the numerical prediction of the interstitial pressure and shear stress is an essential tool to gain a better understanding of the mechanism involved in acupuncture needling.

References

1. Blasselle, A.: Modélisation mathématique de la peau. Thèse de doctorat, Université Pierre et Marie Curie, Paris, France (2011)
2. Decoene, A., Maury, B.: Moving meshes with freefem++. Journal of Numerical Mathematics **20**, 195 (2013)
3. Deleuze, Y., Thiriet, M., Sheu, T.W.H.: Modeling and simulation of local physical stress on the mastocytes created by the needle manipulation during acupuncture. Communications in Computational Physics (2015)
4. Fernández, M.A., Formaggia, L., Gerbeau, J.F., Quarteroni, A.: The derivation of the equations for fluids and structure. In: L. Formaggia, A. Quarteroni, A. Veneziani (eds.) Cardiovascular Mathematics, no. 1 in MS&A, pp. 77–121. Springer Milan (2009)
5. Grandmont, C., Maday, Y.: Fluid-Structure Interaction: A Theoretical Point of View. Revue Européenne des Éléments **9**(6-7), 633–653 (2000)
6. Hecht, F.: New development in FreeFem++. Journal of Numerical Mathematics **20**(3-4), 251 (2013)
7. Park, J.Y., Yoo, S.J., Patel, L., Lee, S.H., Lee, S.H.: Cell morphological response to low shear stress in a two-dimensional culture microsystem with magnitudes comparable to interstitial shear stress. Biorheology **47**(3), 165–178 (2010)
8. Quarteroni, A., Tuveri, M., Veneziani, A.: Computational vascular fluid dynamics: problems, models and methods. Computing and Visualization in Science **2**(4), 163–197 (2000)
9. Raviart, P.A., Thomas, J.M.: Introduction À L'analyse Numérique Des Équations Aux Dérivées Partielles. Masson (1983)
10. Swartz, M.A., Fleury, M.E.: Interstitial Flow and Its Effects in Soft Tissues. Annual Review of Biomedical Engineering **9**(1), 229–256 (2007)
11. Thiriet, M.: Biology and Mechanics of Blood Flows: Part I: Biology. CRM Series in Mathematical Physics. Springer, NY (2008)
12. Thiriet, M.: Cell and Tissue Organization in the Circulatory and Ventilatory Systems, *Biomathematical and Biomechanical Modeling of the Circulatory and Ventilatory Systems*, vol. 1. Springer New York, New York, NY (2011)
13. Thiriet, M.: Cells and tissues. In: Cell and Tissue Organization in the Circulatory and Ventilatory Systems, no. 1 in Biomathematical and Biomechanical Modeling of the Circulatory and Ventilatory Systems, pp. 11–67. Springer New York (2011)
14. Thiriet, M.: Intracellular Signaling Mediators in the Circulatory and Ventilatory Systems, *Biomathematical and Biomechanical Modeling of the Circulatory and Ventilatory Systems*, vol. 4. Springer New York, New York, NY (2013)
15. Thiriet, M., Deleuze, Y., Sheu, T.W.: A Biological Model of Acupuncture and Its Derived Mathematical Modeling and Simulations. Communications in Computational Physics (2015)
16. Tseng, Y.H., Huang, H.: An immersed boundary method for endocytosis. Journal of Computational Physics **273**, 143–159 (2014)
17. Vafai, K., Tien, C.L.: Boundary and inertia effects on flow and heat transfer in porous media. International Journal of Heat and Mass Transfer **24**(2), 195–203 (1981)
18. Wei, F., Shi, X., Chen, J., Zhou, L.: Fluid shear stress-induced cytosolic calcium signalling and degranulation dynamics in mast cells. Cell Biology International Reports **19**(2), 45–51 (2012)
19. Yao, W., Ding, G.H.: Interstitial fluid flow: simulation of mechanical environment of cells in the interosseous membrane. Acta Mechanica Sinica **27**(4), 602–610 (2011)
20. Yao, W., Li, Y., Ding, G.: Interstitial Fluid Flow: The Mechanical Environment of Cells and Foundation of Meridians. Evidence-Based Complementary and Alternative Medicine **2012**, 1–9 (2012)